NASA Technical Paper 2866

1989

Effect of Ephemeris Errors on the Accuracy of the Computation of the Tangent Point Altitude of a Solar Scanning Ray as Measured by the SAGE I and II Instruments

James J. Buglia
Langley Research Center
Hampton, Virginia

National Aeronautics and Space Administration
Office of Management
Scientific and Technical Information Division

Summary

An analysis was made of the error in the minimum altitude of a geometric ray from an orbiting spacecraft to the Sun. The dominant errors result from two sources: determining the position of the spacecraft and determining the position of the Sun.

The sunrise and sunset errors are highly correlated and are opposite in sign. With the ephemeris generated for the SAGE I instrument data reduction, these errors can be as large as 200–350 m (1σ) after 7 days of orbit propagation. The bulk of this error results from errors in the position of the orbiting spacecraft rather than errors in computing the position of the Sun. These errors, in turn, result from the discontinuities in the ephemeris tapes resulting from the orbital determination process. Data taken from the end of the "definitive" ephemeris tape are used to generate the "predict" data for the time interval covered by the next arc of the orbit determination process. The predicted data are then updated by using the tracking data. The growth of these errors is very nearly linear, with a slight nonlinearity caused by the beta angle. An approximate analytic method is given that predicts the magnitude of the errors and their growth in time with reasonable fidelity.

Introduction

A number of scientific reports have recently been cited in the press that describe sundry, sometimes conflicting, scenarios depicting the status and evolution of the ozone content of the Earth's atmosphere. Since ozone effectively filters out most of the potentially harmful ultraviolet radiation from the Sun, the sanctity and preservation of this most important trace gas, and its future in our atmosphere, is obviously of prime importance to all who inhabit this planet.

In October of 1986, the National Aeronautics and Space Administration (NASA), in collaboration with the National Oceanic and Atmospheric Administration (NOAA), the Federal Aviation Administration (FAA), the World Meteorological Organization (WMO), and the United Nations Environmental Panel (UNEP) formed the Ozone Trends Panel. This panel, which consists of more than 100 scientists from all over the world, has been charged with the responsibility for evaluating the sundry findings, which involves the evaluation of ozone measurements from ground-based as well as satellite-borne instruments, and for determining which, if any, of the reported trends, catastrophic or otherwise, are in fact supportable under close scientific scrutiny and examination from a common scientific base.

As a result of the requirements of this panel, detailed error analyses were made of every facet involved in the generation of the final data product from each experiment (each of the analyses was originally reported independently in the technical literature, and some of them led to the press reports mentioned earlier)—e.g., instrument measurement noise and calibration errors and their changes with time, data conversion, and data inversion algorithms—for both the long-established instruments (e.g., Dobson spectrophotometers, rocket sounds) and the more recently developed satellite instruments (SBUV, TOMS, LIMS, MAPS, SAGE I, and SAGE II).

The SAGE I and SAGE II instruments are both used to perform solar occultation experiments in which the instrument scans across the solar disk at sunrise and sunset (with respect to the orbiting satellite) and measures the intensity of the solar radiation as it passes through various depths of the Earth's atmosphere (see, e.g., McCormick 1982, and Mauldin et al. 1985). Scans outside the atmosphere, exoatmospheric scans, provide the reference radiation with which subsequent measurements are ratioed, and hence these instruments are essentially self-calibrating. Scans whose lines of sight pass through the Earth's atmosphere have some of their solar energy removed, either by scattering (Rayleigh and aerosol) or by the absorption of some of this energy by molecules that are optically active in the bandpass of the instrument. The ratios of the atmospheric scans on a given pass to the exoatmospheric scans for the same pass provide a sequence of transmission functions that can be inverted to yield the altitude distribution of the density of the active material (vertical profiles), i.e., of ozone, in the present discussion. These vertical profiles can in turn be integrated to yield the total vertical burden of ozone, for direct comparison with the Dobson data.

Two of the several uncertainties in the data reduction process that affect the accuracy of the end product generated by SAGE I and II are related to the ray that passes from the scan point on the Sun to the instrument—the line of sight, or tangent point ray—namely, (1) the minimum altitude of this ray above the surface of the oblate Earth and (2) the geographic location of this point. These are more fundamentally related to three other questions that arise frequently in orbital mechanics and/or spherical geometry problems:

1. Where is the spacecraft located with respect to a pseudoinertial coordinate system whose origin is at the center of the Earth and whose X-axis coincides

with the vernal equinox (to be defined more precisely later)?

2. Where is the center of the solar disk in the same coordinates?

3. Where is the Greenwich meridian located in the same coordinate system—i.e., what is the Greenwich Sidereal Time?

A first order analysis of the second set of questions, and how these relate to the determination of the tangent point altitude, is the subject of the present paper.

Error Analysis of Ephemeris Data

The SAGE I and II ephemeris data are generated by the Goddard Space Flight Center (GSFC) by using highly sophisticated trajectory computation and orbit determination programs. The spacecraft position and velocity vectors are generated in an inertial coordinate system defined as the mean of 1950.0 coordinates. These data are generated at 1-min intervals (plus other significant event times such as apogee and perigee passage, equatorial crossings). The ephemeris data are generated for a period of 8 days, copied onto magnetic tape and sent to the users at the Langley Research Center (LaRC).

This definitive ephemeris is the result of a number of processes, outlined in flowchart form in figure 1, each of which can inject errors or uncertainties into the final data product.

In the first process, an orbital state vector at some time $t = 0$ is numerically integrated to produce 8 days of ephemeris data at nominally 1-min intervals. The mathematical model used in this step by the GSFC is quite sophisticated and includes many gravitational and nongravitational force terms whose magnitudes have been accurately determined by empirical methods from years of tracking Earth satellites. The resulting orbit is called a "predictive" orbit and represents as good a set of ephemeris data as can be produced a priori by numerically solving the six-dimensional set of differential equations that contain the mathematical model of the force system acting on the satellite.

From the predict orbits, a set of simulated tracking data sets for each station on the tracking network is generated. The position of each tracking station is input as accurately as possible—its latitude, longitude, and distance above or below the reference ellipsoid—and the spacecraft range, range rate, elevation and azimuth angles and their rates, and the spacecraft rise and set times relative to the station are accurately computed.

The stations then proceed to track the actual spacecraft (see fig. 2). The real station tracking data are compared with the predicted data. The differences—called residuals—are then fed into a statistical filter, usually a weighted-least-squares or a maximum likelihood filter, and corrections to the initial conditions computed in such a way that the resulting computed (or modeled) orbit now minimizes some predetermined function of the residuals. This orbit is now called a "definitive" orbit, and it is the one whose ephemeris appears on the GSFC tapes. This represents the best set of orbital data available for the time period spanned by the ephemeris tapes. Because of the way the data are reduced and the ephemeris is computed, the orbit that this process yields is not continuous—there are discontinuities in the orbit state vector from one ephemeris tape to the next. This is shown schematically in figure 3. In the figure, the orbit is depicted as a sequence of disjointed arcs, while in reality each "arc" is about 105 orbits (7 days at approximately 15 orbits per day).

There are three fundmental error sources that produce ephemeris data that deviate somewhat from reality.

1. Imperfect mathematical models: The mathematical model used to generate the predict orbit is necessarily an approximation. Nature is a perfect analogue model, and any attempt to reproduce her results with a finite dimensional numerical model is necessarily going to culminate in only an approximation to the real world situation. Hence, even if the initial conditions of a satellite orbit were perfectly known, the results of the model simulation would immediately begin to deviate from the real state of the satellite and the results would only be of acceptable accuracy until such time as the deviation became perceptible to some measurement process. This time might vary from a few tens of minutes (for a spherical Earth model) to several days or weeks for the GSFC models, depending on the mathematical model used and the purpose for which the ephemeris data are generated.

2. Tracking errors: The tracking hardware used by the on-net tracking stations is subject to both mechanical and electronic errors. These can only track to certain accuracies in range, range rate, and the angular data. The accuracies quoted in the literature for these parameters are a few meters (5–15) in range, 6–30 mm/sec in range rate, 20 arc-sec in angle, and 0.01 arc-sec/sec for angular rates (for angular rates less than about 500 arc-sec/sec).

3. Orbit determination program errors: A complete orbit determination program would be very large, very complex, and very slow. There are many numerical approximations made in the production versions of these programs to speed up the solution process, and these necessarily reduce the accuracy

of the computations to varying degrees. Typical of the types of approximation made are numerical finite difference methods to compute the many partial derivatives used in the inversion, and the linearization of some nonlinear effects. Other small errors are introduced in simplifying some of the mathematical models describing the physical processes occurring in the substructure components (e.g., simple methods of refraction and the effects of the Sun and the Moon on the satellite orbit). Finite word computers also introduce round-off errors which amplify in time.

Determination of Errors in Initial Conditions

The end result of all these errors and uncertainties manifests itself in the following way. The GSFC prepares the definitive orbit tapes and sends these to the working groups at LaRC. Each tape contains 8 days of ephemeris data. The eighth day of one tape is an overlap of the first day of the next tape in the time sequence. The errors mentioned above show up when one compares the individual elements of the state vectors at the same times from these overlapping data sets.

At the time the present study was initiated, there were 139 such overlaps on tapes containing SAGE I ephemeris data and 49 overlaps on the SAGE II tapes. The state vectors corresponding to the same data and time of day for each of the 139 SAGE I tapes were differenced, and the differences formed into a variance-covariance matrix according to the following standard maximum-likelihood estimator:

$$\begin{aligned}\mathrm{cov}(\Delta \mathbf{r}) &= E[(\mathbf{r}_8 - \mathbf{r}_1)\ (\mathbf{r}_8 - \mathbf{r}_1)^T] \\ &= \frac{1}{N}\sum_{i=1}^{N}(\mathbf{r}_{8_i} - \mathbf{r}_{1_i})(\mathbf{r}_{8_i} - \mathbf{r}_{1_i})^T \qquad (1)\end{aligned}$$

where $\mathbf{r}_8$ is the state vector at the beginning of day 8 of one tape, $\mathbf{r}_1$ is the state vector at the corresponding time from day 1 of the next tape, and $\Delta \mathbf{r} = \mathbf{r}_8 - \mathbf{r}_1$. For SAGE I, $N = 139$, and for SAGE II, $N = 49$. This procedure resulted in the following set of standard deviations in the state vector:

	SAGE I	SAGE II
σ_x, m	326.0	195.7
σ_y, m	391.0	172.5
σ_z, m	281.4	127.4
$\sigma_{\dot{x}}$, m/sec	0.35	0.18
$\sigma_{\dot{y}}$, m/sec	0.32	0.10
$\sigma_{\dot{z}}$, m/sec	0.39	0.21

The reason for the apparent improvement in the SAGE II data is that in generating the 8-day tape for SAGE I a full 8 days of tracking data were processed and a definitive orbit was determined for the full time span. In the SAGE II processing, two separate 4-day definitive orbits were computed independently and placed on one 8-day tape. From here on, only SAGE I results will be discussed, with the reasonable assumption that the SAGE II results will be about half those for SAGE I (see appendix A).

It is not possible to determine what proportion of these errors comes from errors in the state vector of day 7 of the first tape and how much comes from day 1 of the next tape. It is, therefore, assumed here that the actual errors at the beginning of day 1 of any tape are very small and that essentially all the error accumulated at day 7 of a given tape is a result of small errors at day 1 being propagated forward through 7 days of time. The only justification for this assumption, as will be shown, is that the error growth at the end of a 7-day period is rather close to the magnitude of the errors observed in the above-mentioned comparison of the state vector. Note that 7 days of propagation time is used, as $t = 0$ of a given tape is equivalent to the beginning of day 8 of the previous tape, which occurs at the end of the 7th day plus one orbit.

The next step is to determine what values of the standard deviations in the uncertainties of the initial conditions are required at $t = 0$ such that the above values of uncertainties are realized after 7 days of error propagation. One of the SAGE I tapes was picked arbitrarily, and the initial conditions at $t = 0$ of day 1 were assumed to represent nominal conditions. An initial set of standard deviations was assumed and a random number generator used to determine 20 sets of initial conditions for a set of perturbed orbits. Each of these were run out for the full 7 days, and each hour the differences between the perturbed and nominal orbits were collected. The means and standard deviations were computed at each hour and the results plotted. The initial guess at the standard deviations in the initial conditions was adjusted until the standard deviations of the state vector elements after 7 days agreed reasonably well with the table above, computed from the real ephemeris data. These standard deviations at $t = 0$ were found to be

$$\begin{aligned}\sigma_{x_o} &= 0.3227 \text{ m} \\ \sigma_{y_o} &= 0.3870 \text{ m} \\ \sigma_{z_o} &= 0.2781 \text{ m} \\ \sigma_{\dot{x}_o} &= 0.3465 \times 10^{-3} \text{ m/sec} \\ \sigma_{\dot{y}_o} &= 0.3168 \times 10^{-3} \text{ m/sec} \\ \sigma_{\dot{z}_o} &= 0.3861 \times 10^{-3} \text{ m/sec}\end{aligned}$$

Figure 4 shows a typical plot of the resulting history of the x-component of the state vector errors. It is seen that the midpoint of the oscillation at $t = 168$ hr (7 days) is very close to the 326 m called for (see also appendix B).

The next step, using the standard deviations at $t = 0$ just found, was to generate a number of perturbed orbits and compute statistics on the pertinent parameters. A sample size of 100 was chosen here and the parameters whose statistics were generated were

1. The difference between the tangent point altitudes at sunrise for the perturbed and nominal orbits. The nominal altitude chosen here was 10 km. A few check runs showed that the altitude difference was essentially independent of the magnitude of the nominal altitude.
2. The same as above for the sunset events.
3. The difference between the sunrise tangent point altitude and the very next sunset tangent point altitude on the same orbit.

The rise and set altitudes were determined as follows. The initial conditions were taken from the SAGE I ephemeris tapes. These initial conditions were assumed to be a nominal set for the beginning of each 7-day period. For a nominal tangent point altitude of 10 km, the time of every rise and set event during the ensuing 7-day period was computed from a program based on Buglia (1986) and written to a data file, along with the β angle (see fig. 5) at each event time. The nominal initial conditions were then fed into a second program which, using a random number generator, computed 100 sets of random initial conditions, Gaussian distributed with zero mean and standard deviation given above for $t = 0$. A third program then computed the tangent point altitudes for each rise and set event for each orbit for the same times as determined for the nominal orbit (see fig. 6). For each of the 100 perturbed orbits, the three statistics described above were determined for each event and the results plotted.

The entire process was repeated for 25 consecutive weeks in order to get a reasonable variation of the β angle into the results. As shown in figure 5, β is the angle between the direction to the Sun and the orbital plane, measured positive in the direction of the angular momentum vector of the orbit. For $\beta = 90°$ (a situation not encountered on either SAGE I or SAGE II, the maximum useful value of β for the SAGE instruments is about 66°), the orbital plane is normal to the Sun direction, and it is apparent that even a large error along the orbit will have little effect on the altitude of the tangent point altitude. For $\beta = 0°$, on the other hand, the Sun "sees" the orbit edge-on, and here small errors along the orbit path will result in large errors in tangent point altitude. Figure 5 shows this $\beta = 0°$ situation more clearly, and this is the geometry that would produce the maximum error in tangent point altitude.

A few histograms were plotted showing the distribution of the quantity $(h_R - h_{NR})$, where h_R is the rise altitude of the perturbed orbit and $h_{NR} = 10$ km, the nominal rise altitude. Two of these are presented in figures 7 and 8, showing that with only a little imagination these appear to be normally distributed with essentially zero mean. Two cases with extreme variation were chosen here for display purposes. The distributions are thereby assumed normal, and hence it makes sense from here on to characterize their distributions by use of standard deviations.

The standard deviation histories of the three quantities mentioned earlier are shown from a typical run on the next three figures, figures 9–11. These are the standard deviations in the quantities $(h_R - h_{NR})$, $(h_S - h_{NS})$, and $(h_R - h_S)$, where h_S is the set altitude and $h_{NS} = 10$ km, the nominal set altitude. The statistic $(h_R - h_S)$ does not include any nominal data (except implicitly in the time, of course) but is the difference between the rise altitude and the very next set altitude in the same perturbed orbit.

These curves are typical of the histories of the noted statistical quantities for small to moderate variations in the β angle (the effects of β will be shown later). In these figures, β increases from –33° at $t = 0$ to about –4° at $t = 168$ hr. The standard deviation increases from some very small—but not zero—value at $t = 0$ to something of the order of 340 m for both $(h_R - h_{NR})$ and $(h_S - h_{NS})$ (figs. 9 and 10) and to about twice this (as expected) for the quantity $(h_R - h_S)$ (fig. 11), and this increase is very nearly linear (see appendix A).

Much of the effect of errors in the initial coordinates manifests itself as a very small error in the mean angular velocity of the spacecraft and consequently shows up as a displacement error along the flight path in the nominal orbit plane. As shown in appendix A, for zero β angle, the angle between the nominal and perturbed radius vectors at time t is given approximately by

$$\theta \approx \left[\frac{3}{2}\left(\frac{\mu}{a^3}\right)^{1/2}\frac{\Delta a}{a}\right]t \qquad (2)$$

where a is the semimajor axis of the nominal orbit and μ is the gravitational constant for the Earth, 398 600.64 km^3/sec^2. For example, for the orbits of figures 9–11, $a = 6963$ km and for a moderate $\Delta a = 0.001$ km, the above equation gives an angle θ after 7 days of 1.415×10^{-4} rad. This yields in

a down-track error of just under 1 km. From the relation (appendix A)

$$\Delta h = -\left(r_{sc,N} \cos \phi_N\right) \theta \qquad (3)$$

one computes a rise and set altitude error of about 390 m, which is somewhat higher than that shown in figures 9–10 but is the correct order of magnitude and is very close in magnitude to some of the standard deviations computed for other time periods. Figure 12 shows that for nearly circular orbits, a "fast" timing error would cause an increase in the sunrise altitude and a corresponding decrease, of about the same magnitude, in the sunset altitude. This is borne out in the figures and is also obviously the reason why the error in the difference $(h_R - h_S)$ is about twice the error in either sunrise or sunset altitude. This also indicates that the rise and set altitude difference should be highly correlated from one orbit to the next, and this is amply illustrated in figure 13, which shows a time history of $(h_R - h_S)$ for one of the 100 perturbed orbits used in the statistical data compilation. For this particular choice, this quantity is negative over the entire period and the high degree of correlation between orbits is shown clearly—given a few hours history of this difference, the difference for the next few days is quite predictable. It is important to emphasize this fact that, starting with a given ephemeris tape from the GSFC, a bias will develop between the calculation of the rise and set altitudes and that this bias will increase approximately linearly over the 7–8 days of computation time. For the example shown, this bias grew to about 700 m in 7 days, the computed set altitude being higher than the computed rise altitude (at the nominal times), indicating a fast time error (the semimajor axis of the computed orbit is slightly smaller than the (unknown) semimajor axis of the real orbit).

The variation of the altitude error with the β angle is shown in figure 14. The standard deviation of the quantity $\sigma(h_R - h_S)$ is shown in the upper half of the figure and that for $\sigma(h_R - h_{NR})$ is shown in the lower half, both plotted against β, at $t = 168$ hr for each of the 25 weeks of data. To get the point at $\beta = 0°$, the mean of the quantity $\sigma(\Delta h)/\cos \beta$ was computed using the results at $t = 168$ hr. The solid curves are then plots at $A \cos \beta$, where A is the amplitude for each of the statistics described above.

Solar Ephemeris Errors

A number of procedures were used in the SAGE I and II data reduction algorithms to accurately compute the position of the center of the solar disk with respect to the center of the Earth and subsequently with respect to the orbiting spacecraft. The coordinate system chosen for all subsequent calculations is the mean of date system, in which the X-axis (the vernal equinox) is determined by the intersection of the Equator with the ecliptic, precession being taken into account (nutation is neglected). The scan plane of the SAGE instruments contains the spacecraft and the centers of the Earth and the Sun. The positions of the top and the bottom of the Sun as seen in the scan plane are computed, with due allowance made for the refraction of the ray as it passes through the atmosphere. The algorithms ultimately developed are completely self-sufficient in that they do not need any external ephemerides or other input—the only inputs needed are a calendar date and a Greenwich Mean Time, and the corresponding position and velocity vectors of the spacecraft.

All the equations and methods used in these algorithms, except the aberration corrections, are outlined and discussed in Buglia (1988).

Definition of Minimum Altitude

Assume a quasi-inertial coordinate system with the origin at the center of the Earth (fig. 15). The Z-axis is along the rotational axis of the Earth, and the equatorial plane passes through the origin and is normal to the Z-axis. The X-axis, or vernal equinox, is located by definition as the point on the equatorial plane where the geocentric orbit of the Sun crosses the Equator from south to north. This occurs about 21 March of each year. The Y-axis lies also in the equatorial plane in such a way as to complete a right-hand system. This is called a quasi-inertial system because the vernal equinox is not fixed in inertial space, but moves slowly with time (the precession of the equinox—see, e.g., Buglia 1988).

The mathematical shape describing the surface of the Earth (sphere, oblate spheroid, geoid) is given in this coordinate system. Also given are three position coordinates and three velocity coordinates of an orbiting spacecraft at some specific time, and the three position coordinates of some celestial body (in this study, the center of the disk of the Sun), both relative to the Earth-centered inertial system. From these parameters one can define a vector pointing from the spacecraft to the celestial body. If one starts at the spacecraft and makes one's way along this vector, or ray, and looks vertically downward (in the plane formed by the centers of the three objects—the centers of the Earth, Sun, and spacecraft), one finds that a minimum altitude above the Earth's surface occurs somewhere along this ray. The point on the ray at which this minimum occurs is called the *tangent point*, and the point on the surface of the Earth immediately below the tangent point is called,

appropriately enough, the *subtangent point.* The distance between the tangent point and the subtangent point is the altitude of the tangent point and is the minimum altitude referred to in the remainder of the present paper. The computation of the minimum height is trivial for a spherical Earth, but gets a bit more complicated when made for an oblate spheroid (see, e.g., Buglia 1988). A subroutine in the SAGE I and II data reduction software computes the magnitude of this minimum distance and the inertial coordinates of the subtangent point. The geographic coordinates (ordinary geodetic latitude and longitude) are also computed.

Error Sources in Minimum Height Calculation

It can be seen from the above definition of the tangent point that there are three major geometric sources that contribute to errors in determining the minimum height of the observation ray above the Earth's surface and two additional corrections that have to be made to yield the position of the Sun as seen at the spacecraft. The geometric error sources are

1. The shape assumed for the surface of the Earth.
2. Uncertainties in the geocentric position of the spacecraft.
3. Uncertainties in the geocentric position of the center of the Sun.

The additional corrections that need to be made are

4. Planetary aberration due to the motion of the Earth around the Sun.
5. Orbital aberration due to the motion of the spacecraft around the Earth.
6. Atmospheric refraction. Uncertainties due to refraction uncertainties were not included in the present paper. See Chu 1983.

1. Shape of the Earth. For a point on the surface of the rotating Earth, the potential of gravity, W, is the sum of the potential of the gravity force (due to the mass distribution of the Earth) and the centrifugal potential (due to the rotation of the Earth) (see, for example, Heiskanen and Moritz 1967, ch. 2)

$$W = \frac{\mu}{r}\left\{1 - \sum_{n=1}^{\infty}\sum_{m=0}^{n}\left(\frac{a_e}{r}\right)^n P_{nm}(\sin\theta) \times [J_{nm}\cos(m\lambda) + K_{nm}\sin(m\lambda)]\right\} + \frac{1}{2}\omega_e^2 r^2\cos^2\theta \quad (4)$$

in which

μ	Earth gravity constant, 398 600.64 km^3/sec^2
r	geocentric radius to a point on the surface, km
a_e	equatorial radius of the Earth, 6378.1600 km
θ	geocentric latitude, deg
λ	longitude from Greenwich, deg
ω_e	angular velocity of the Earth's rotation, $7.292\,115\,855 \times 10^{-5}$ rad/sec

where P_{nm} are the standard associated Legendre polynomials, and J_{nm} and K_{nm} are integrals involving the mass distribution of the Earth. These are the gravitational constants mentioned earlier. These have been empirically determined by the GSFC from satellite tracking.

For the SAGE I and II software, the assumption was made that the potential of gravity was rotationally symmetric about the north polar axis. This removes the longitudinal dependence from equation (4) and allows it to be written in the simpler form involving only zonal harmonics

$$W = \frac{\mu}{r}\left[1 - \sum_{n=2}^{\infty}\left(\frac{a_e}{r}\right)^n J_n P_n(\sin\theta)\right] + \frac{1}{2}\omega_e^2 r^2\cos^2\theta \quad (5)$$

This dynamical form was used in some of the SAGE software, with the first six zonal harmonics being

$$J_1 = 0$$
$$J_2 = 1082.6271 \times 10^{-6}$$
$$J_3 = -2.5358868 \times 10^{-6}$$
$$J_4 = -1.6246180 \times 10^{-6}$$
$$J_5 = -0.22698599 \times 10^{-6}$$
$$J_6 = 0.54518572 \times 10^{-6}$$

The radius of the constant potential surface represented by equation (5) was computed for the Earth's surface potential (from eq. (5) at the Equator) and compared with the radius computed from a simple ellipsoid with equatorial radius of 6378.160 km and polar radius of 6356.775 km. These are shown in comparison in the table on the following page. It is seen that the maximum difference occurs at 45° latitude and is less than 82 m. This was considered small, and in all the algorithm segments involving

θ, deg	r_e (ellipsoid), km	r_w (potential), km	$r_w - r_e$, m
0	6378.14000	6378.14000	0
5	6377.97906	6377.97485	−4.21
10	6377.50100	6377.48831	−12.69
15	6376.72000	6376.69553	−24.47
20	6375.65925	6375.62110	−38.15
25	6374.35033	6374.29822	−52.11
30	6372.83230	6372.76760	−64.69
35	6371.15063	6371.07617	−74.46
40	6369.35588	6369.27554	−80.33
45	6367.50223	6367.42048	−81.75
50	6365.64588	6365.56719	−78.69
55	6363.84337	6363.77170	−71.67
60	6362.14980	6362.08819	−61.61
65	6360.61717	6360.56740	−49.77
70	6359.29271	6359.25517	−37.54
75	6358.21737	6358.19105	−26.31
80	6357.42447	6357.40715	−17.31
85	6356.93864	6356.92714	−11.50
90	6356.77500	6356.76550	−9.50

the geometric Earth surface the ellipsoid of revolution was used in place of the surface defined by the harmonic potential. The quoted values of the ellipsoidal radii, the J-coefficients, and the gravitational constant are the latest (as of March 1986) received from the GSFC. These data are for the Northern Hemisphere only. There is no north-south symmetry because of the nonvanishing of the odd-J terms (the J_3 term, for example, gives the "pear shape" to the Earth). The difference in Earth radius at the corresponding north-south latitudes may be as high as 30–35 m, but in no case does the potential surface radius described from equation (5) deviate by more than 80 m or so from that of the ellipsoid.

2. Errors in the position of the orbiting spacecraft. The spacecraft ephemeris computations are made in the data reduction software package by numerically integrating the equations of motion of the spacecraft in a quasi-inertial coordinate system fixed at the center of the Earth. The gravity field used in the model is the sixth-order zonal model described above.

Ephemeris data, deduced from actual spacecraft tracking data, are received from the GSFC on magnetic tapes as discussed earlier. These data are given at nominally 1-min intervals in the mean 1950.0 coordinate system and span an 8-day time interval. The adjective "mean" here is the standard astronomical meaning and indicates that the precessional effect of the Earth's rotation has been included in the coordinate computation, but the nutational effects have not. The initial conditions for the ephemeris integration are extracted from this tape for the time corresponding to the nearest minute of time preceding the beginning of the data taking event. The initial state vector is transformed from the mean 1950.0 coordinates to the mean of date coordinates, the date as specified on the GSFC tape, using the standard transformation equations of spherical astronomy (see, for example, Taff 1985). The equations of motion are then integrated in this coordinate system at 60 equal time intervals throughout the data taking period, which generally ranges from 70–90 sec.

Near a graze event (β near 66°) the tangent height decreases toward zero as the Sun begins to set, just touches the horizon, and immediately begins to increase as the Sun rises. These events may last as long as 10–12 min. Even for this length of time, the root sum square differences between the position and velocity vectors as computed from the zonal-only model described above and the GSFC results, accepting the GSFC results as a standard, are only of the order of 10 m and 20 mm/sec, respectively. These differences are deemed quite acceptable.

3. Solar ephemeris calculations.. The computation of the geocentric position of the center of the Sun for any day of any year, and any time of day, is accomplished by the use of highly accurate series expressions that give the mean longitude, mean anomaly, and true anomaly of the Sun, and the eccentricity of the Earth orbit, all computed with respect to the

mean equator and equinox of date (see algorithms in Buglia 1988). These allow the computation of the right ascension and declination of the center of the Sun with respect to the mean equinox and equator of date.

In a similar way, the Mean Greenwich Sidereal Time is computed from formulas that give the MGST at 0 hr GMT for any date and are then corrected for time of day.

4. Planetary aberration. There is a slight shift in the position of the Sun as seen at the Earth's center because of the finite speed of light. It takes about 8.3 min for photons from the Sun to reach the Earth, so we really see the Sun where it was 8 min earlier. The ratio of the Earth's orbital speed (30 km/sec) to the speed of light (300 000 km/sec) is about 0.0001, and since the Earth's velocity is essentially normal to the Earth-Sun line, the maximum displacement in the solar position due to planetary aberration is of the order of 20 arc-sec. Most of this shows up as an essentially constant decrease of 20 arc-sec or so in the right ascension of the Sun, with a periodic shift in declination of amplitude 9 arc-sec and period one year. This correction is made in the SAGE I and II software by using the classical aberration correction formulas of spherical astronomy (e.g., Smart 1977). The correction as applied here is the reverse of that usually made in classical astronomy. There, the correction is applied to the "observed" coordinates to yield the "true" position. Here, the "true" coordinates are calculated, and the correction is added to yield the "observed" position.

5. Orbital aberration. In addition to the Earth orbital motion about the Sun, the spacecraft orbiting about the Earth introduces an additional aberration effect due to its own velocity. To be strictly correct, the velocities of the spacecraft with respect to the Earth and that of the Earth with respect to the Sun should be added vectorially, and the component of this resultant normal to the line of sight from the spacecraft to the Sun used to compute the total aberration effect, which is then apportioned among the right ascension and declination in accordance with the classical formulas.

In the SAGE I and II software, the orbital aberration has been neglected. The orbital velocity of the spacecraft is approximately 7.5 km/sec. This is about one-fourth of the orbital velocity of the Earth, and hence the maximum aberration shift caused by the orbital motion would be about 5 arc-sec. However, this maximum value would only be realized if the spacecraft were traveling in a direction normal to the Earth-Sun line. In fact, however, during periods of observation of sunrise and/or sunset, the spacecraft is traveling essentially in a direction toward or away from the Sun, a condition that minimizes the aberration shift. Even during the graze events, when the plane of the spacecraft is as nearly normal to the Earth-Sun line as it gets during observations, the displacement due to aberration is of the order of 2 arc-sec. The other extreme case occurs when the orbital plane contains the Earth-Sun line and the Sun is on the Earth horizon. The angle between the velocity vector and the Earth-Sun line is about 24°, and this produces an aberration shift of about 3 arc-sec. Now, 1 arc-sec angular displacement at the spacecraft produces an altitude error of about 14 m, and hence the maximum altitude error due to neglect of their orbital aberration is only about 40 m.

Accuracy of Computations of Coordinates of Sun Center

To check the accuracy of these computations, a number of calculations were made with the software and compared with appropriate data in the Astronomical Almanacs for a number of years.

The Mean Greenwich Sidereal Times and the apparent right ascension and declination of the center of the Sun were extracted from the pertinent Astronomical Almanacs for 0 hr GMT for the first of each month for the years 1979–1987 inclusive.

The Greenwich Sidereal Time calculations were found to be very close. The computed mean sidereal times differed from the published values by only 0.001–0.002 sec for the years 1979–1983. From 1984 to 1987 the difference between the computed and published times jumped to 0.070 sec and remained fixed for these years. The reason for this change is that in 1984 the International Astronomical Union adopted, among other resolutions, the following changes in their procedures for computing ephemerides:

1. A new standard equinox (Jan 1.5, 2000 instead of Jan 0.5, 1900).
2. A more accurate and self-consistent set of planetary masses.
3. Small corrections to the precession/nutation constants.
4. General relativity is now included in the equations of motion of the planetary orbits.

The new constants are now included in the computation of the SAGE ephemeris parameters for the years 1984+, and the differences between the computed and published Greenwich Sidereal Times are now again down in the 0.001–0.002 sec range.

The differences between the computed and published coordinates of apparent right ascension and declination are shown graphically in figures 16 and 17,

respectively. These data are plotted for the first day of each month for the years 1979–1987, inclusive.

The mean (average) error in the right ascension is 5.4 arc-sec, with a standard deviation of 9.6 arc-sec. The corresponding quantities for the declination are –0.7 arc-sec and 5.0 arc-sec. Since both of these uncertainties are transcendentally related to uncertainties in the tangent point height, it is perhaps more useful—and certainly more extreme—to consider the root sum square of these errors and assume that this result acts directly in the direction of maximum tangent point altitude error. Figure 18 displays this parameter for the same conditions as stated earlier. The mean uncertainty here is 10.3 arc-sec with a standard deviation of 8.5 arc-sec. Even if all this error acted in the scan direction (which, as stated above, it does not), the resultant uncertainty in the tangent point altitude would be 147 ± 116 m (1σ).

Thus, in an absolutely worst case scenario, if all of the above uncertainties acted together in the worst way, the mean uncertainty in the tangent point height due to uncertainties in the computation of the solar position would be 147 + 116 + 40 or 303 m. Considering that the errors attain their maxima at different times and that they act in different directions, it is reasonable to conclude that the most likely uncertainties due to ephemeris error are considerably less than 303 m, perhaps a factor of 5–10 less.

Conclusions

The results of the present study of ephemeris errors contained on the SAGE I ephemeris tapes obtained from the GSFC permit the following conclusions to be drawn:

1. The accuracy of the ephemeris tapes is at worst several hundred meters, and it is doubtful that much improvement could be realized by the GSFC.
2. The standard deviation in the error between the true (but unknown) rise and set tangent point altitudes and those computed from the GSFC ephemeris tapes for SAGE I can amount to as much as 200–350 m at the end of 168 hr of error propagation.
3. The rise and set tangent point errors are generally of opposite sign and equal in magnitude (for the nearly circular orbits of SAGE I), so that the standard deviations in the difference between the rise and set tangent point heights is about twice that for the individual errors, or about 400–700 m.
4. On a given orbit, the rise and set tangent point altitude errors are always of about the same order of magnitude (for the nearly circular orbits of SAGE I) and are always opposite in sign. The sign persists, at least over the 7 days studied here, and the magnitudes vary essentially linearly with time. There is, therefore, a very high degree of correlation between these altitudes over the time span covered by a single ephemeris tape.
5. The uncertainties introduced in the computation of the tangent point altitudes due to uncertainties in determining the position of the spacecraft and the position of the Sun in the appropriate coordinate system are considerably smaller than those due to the spacecraft ephemeris computation errors. A worst case scenario, totally at variance with physical reality, indicates that this error should be smaller than about 300 m, with the real world error probably being one-half to one order of magnitude smaller than this.

NASA Langley Research Center
Hampton, VA 23665-5225
December 8, 1988

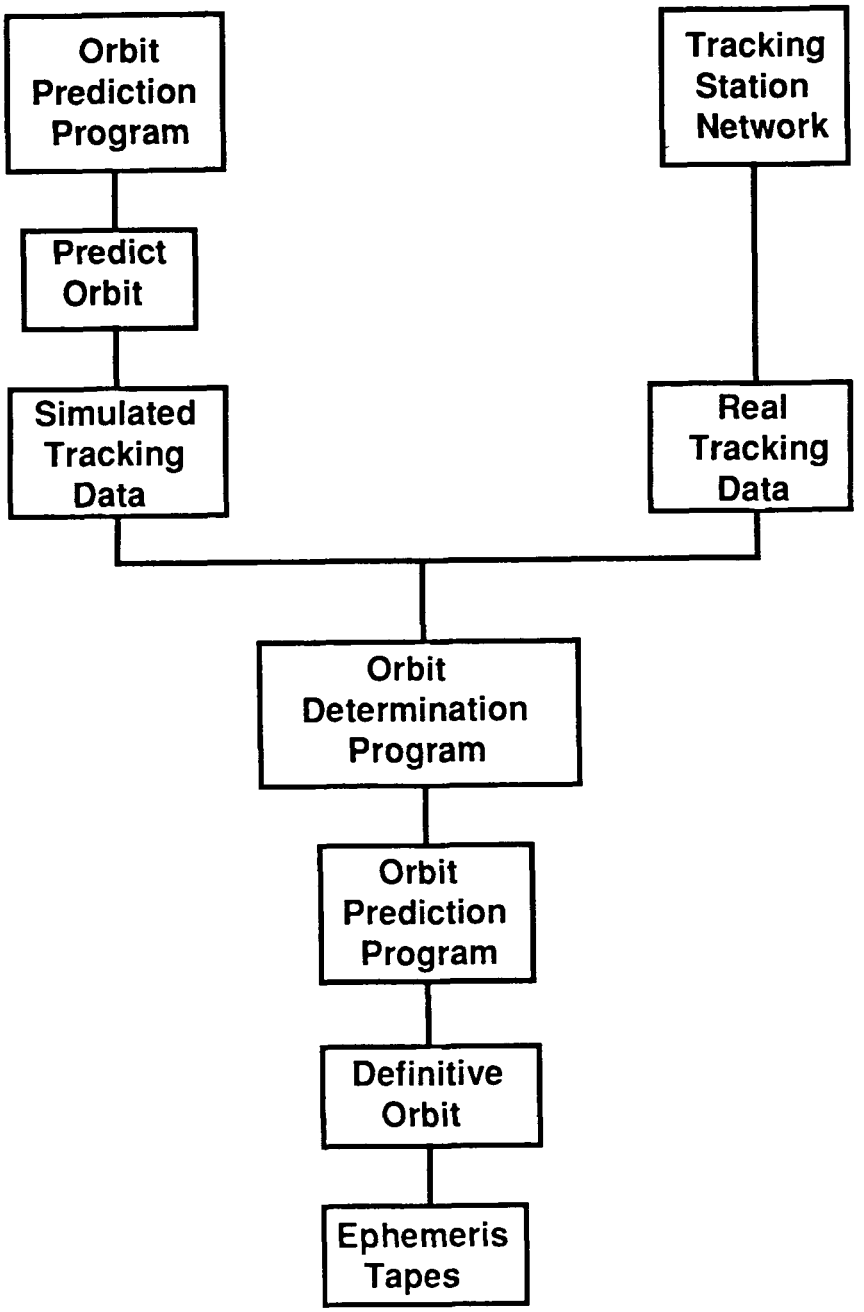

Figure 1. Schematic of the process leading to the generation of SAGE I and II ephemeris tapes.

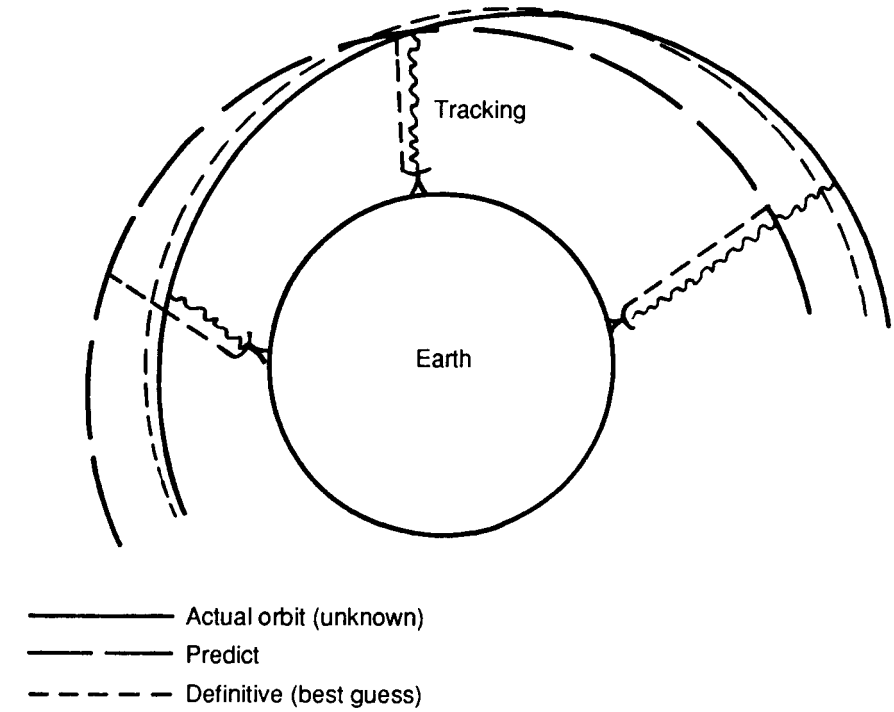

Figure 2. Illustration of the three orbits: actual, predict, and definitive.

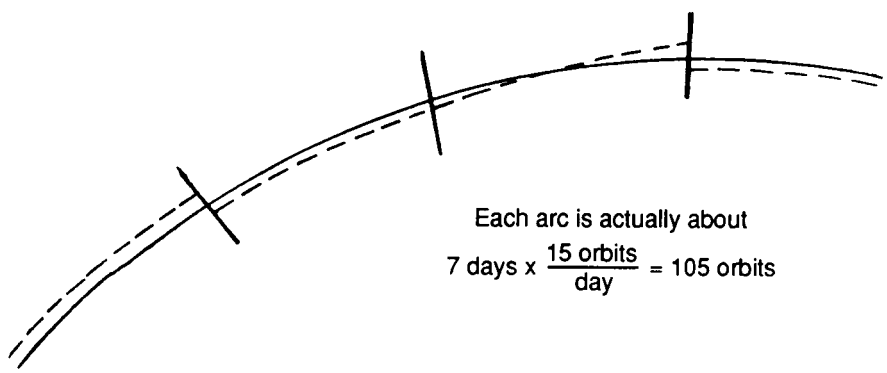

Figure 3. Discontinuities between weekly ephemerides.

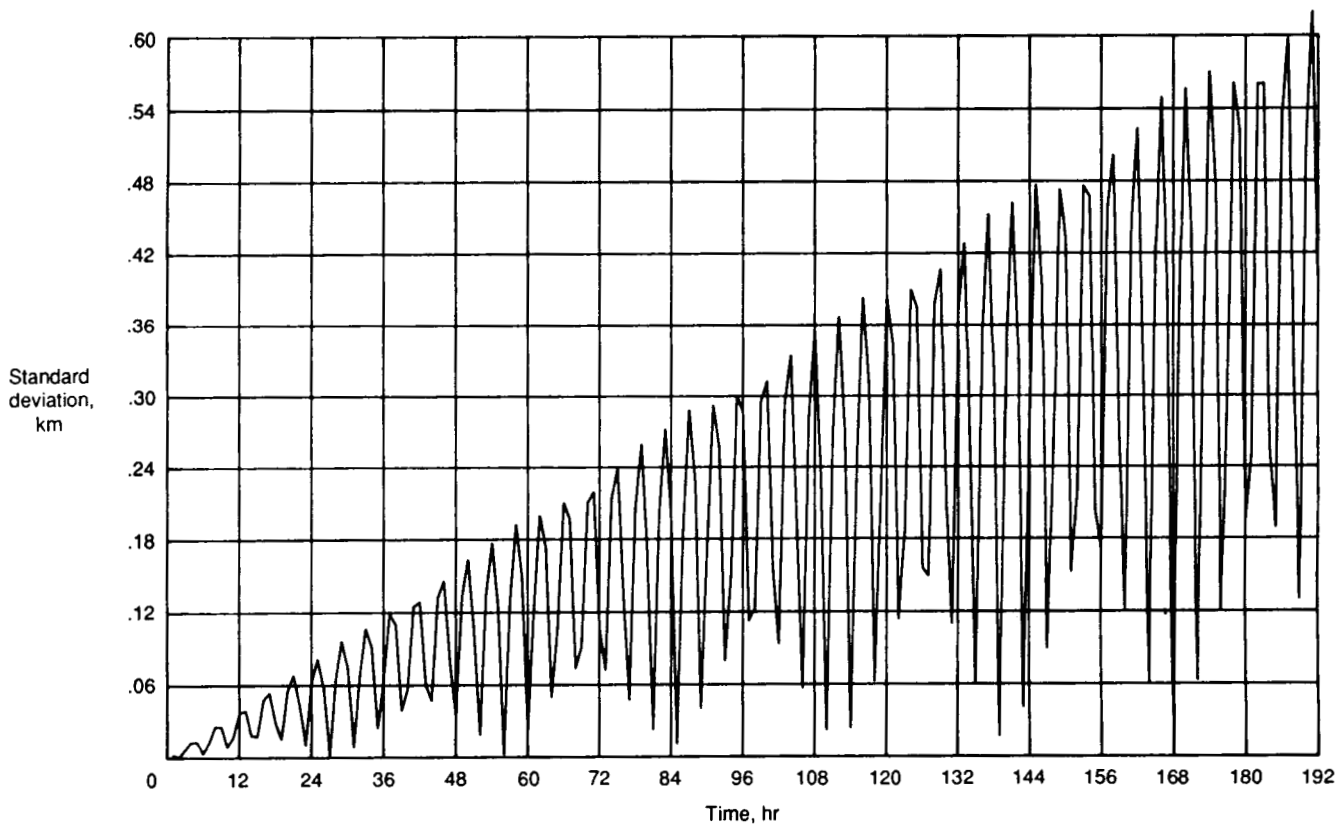

Figure 4. Propagation of the standard deviation in the x-component of the state vector resulting from application of the text standard deviations at $t = 0$.

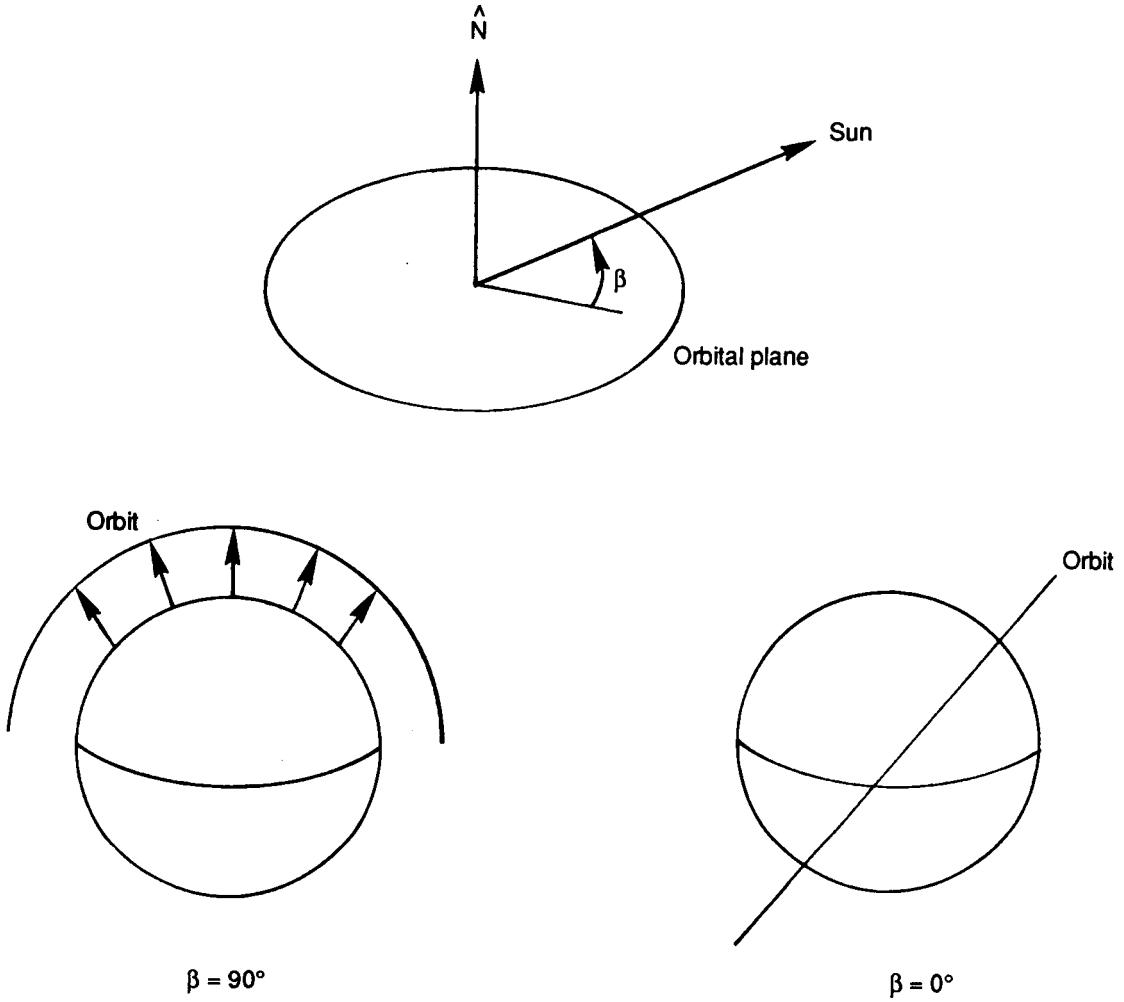

Figure 5. Definition of β angle with extremes of $\beta = 0°$ and $\beta = 90°$ as seen from the Sun. $\hat{N}$ is a unit normal to the orbital plane.

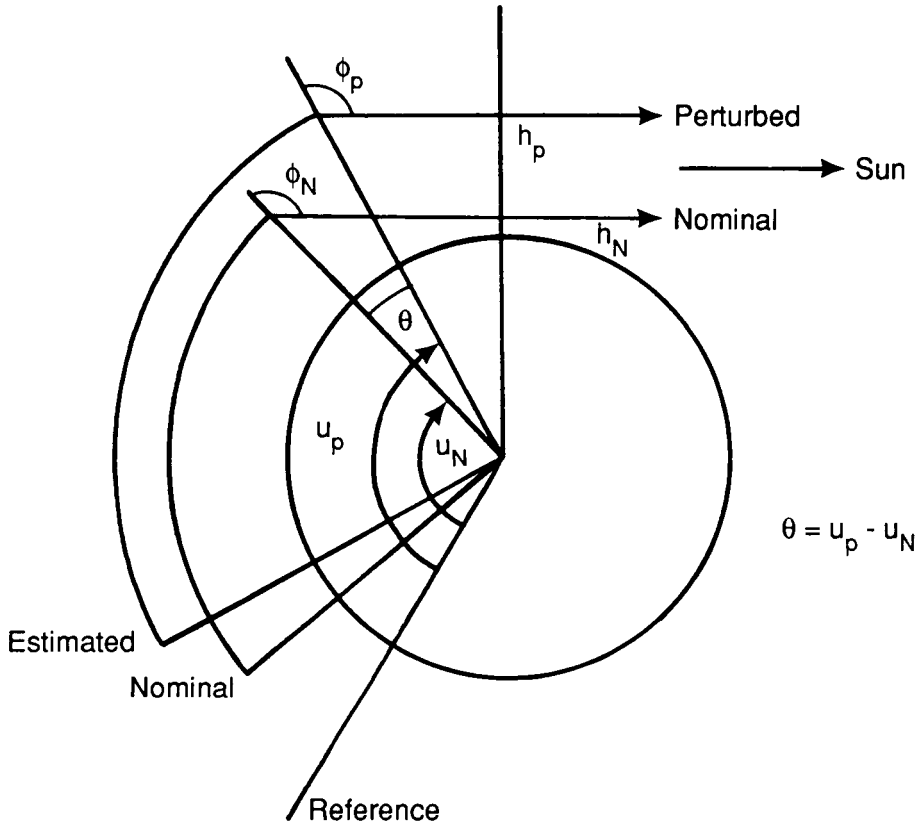

(a) Detailed sketch.

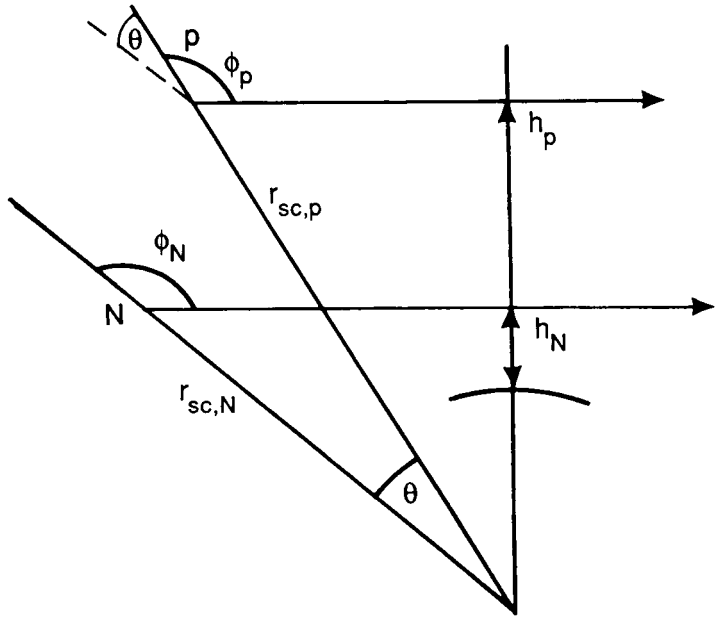

(b) Enlargement of area around tangent point.

Figure 6. Sketch showing the computation of the sunrise tangent point altitude error.

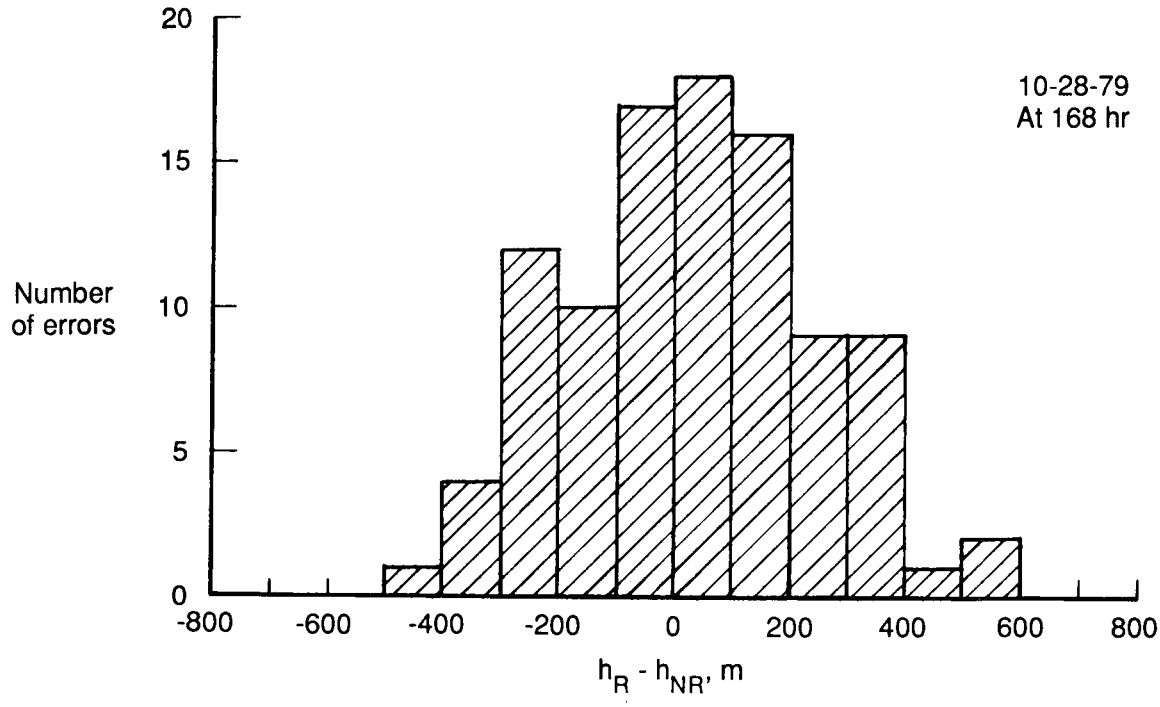

Figure 7. Histogram of the errors in sunrise tangent point altitude at 168 hr using the ephemeris tape for the week of 10/28/79.

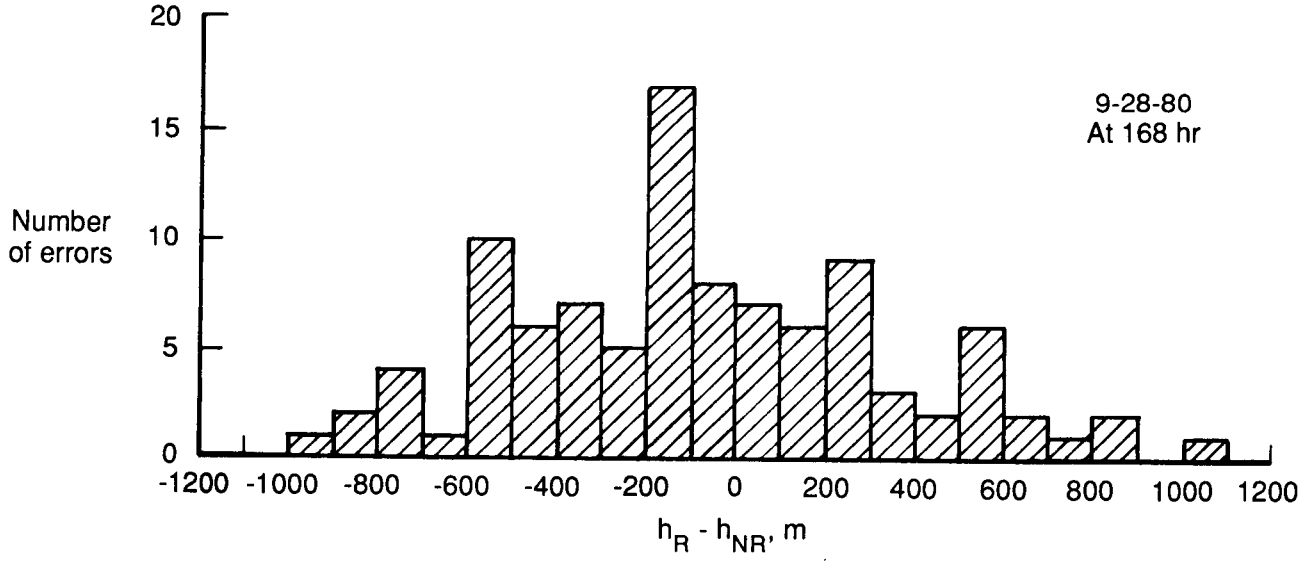

Figure 8. Histogram of the errors in sunrise tangent point altitude at 168 hr using the ephemeris tape for the week of 9/28/80.

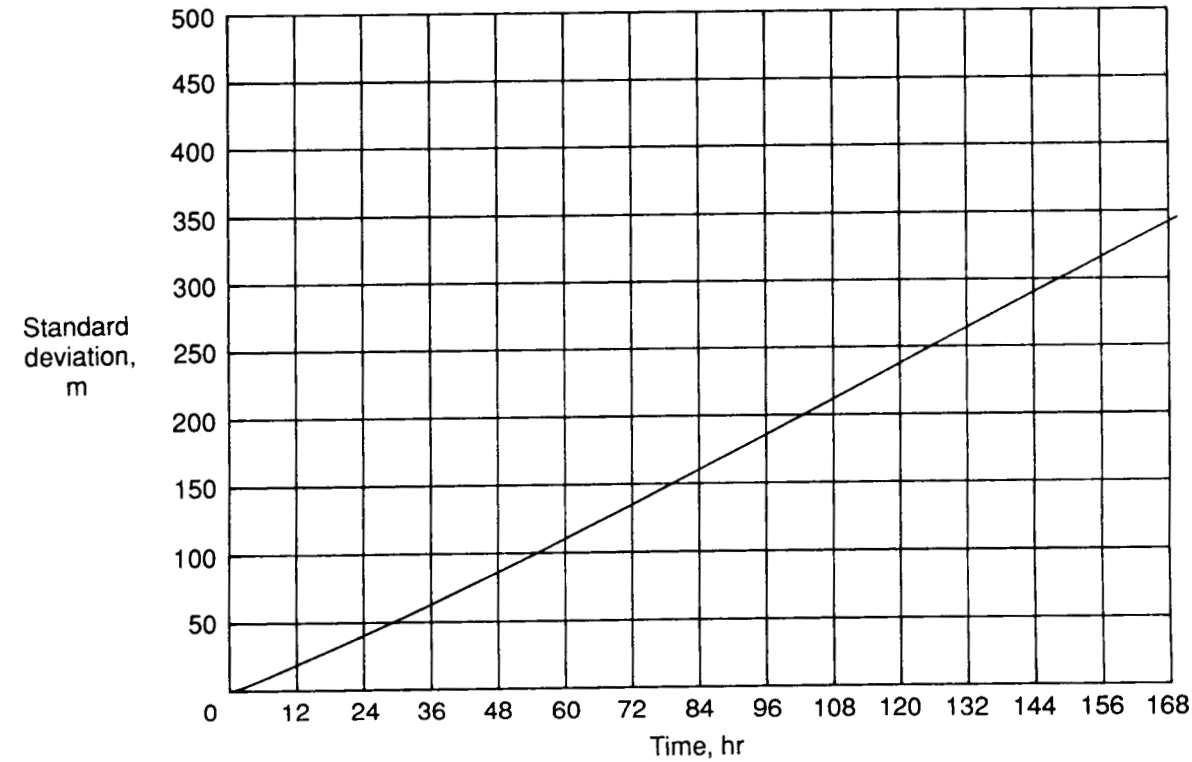

Figure 9. History of the standard deviation in the sunrise altitude error for the week of 11/25/79. The magnitude of the β angle decreases from 33° to 4° during the 7-day period.

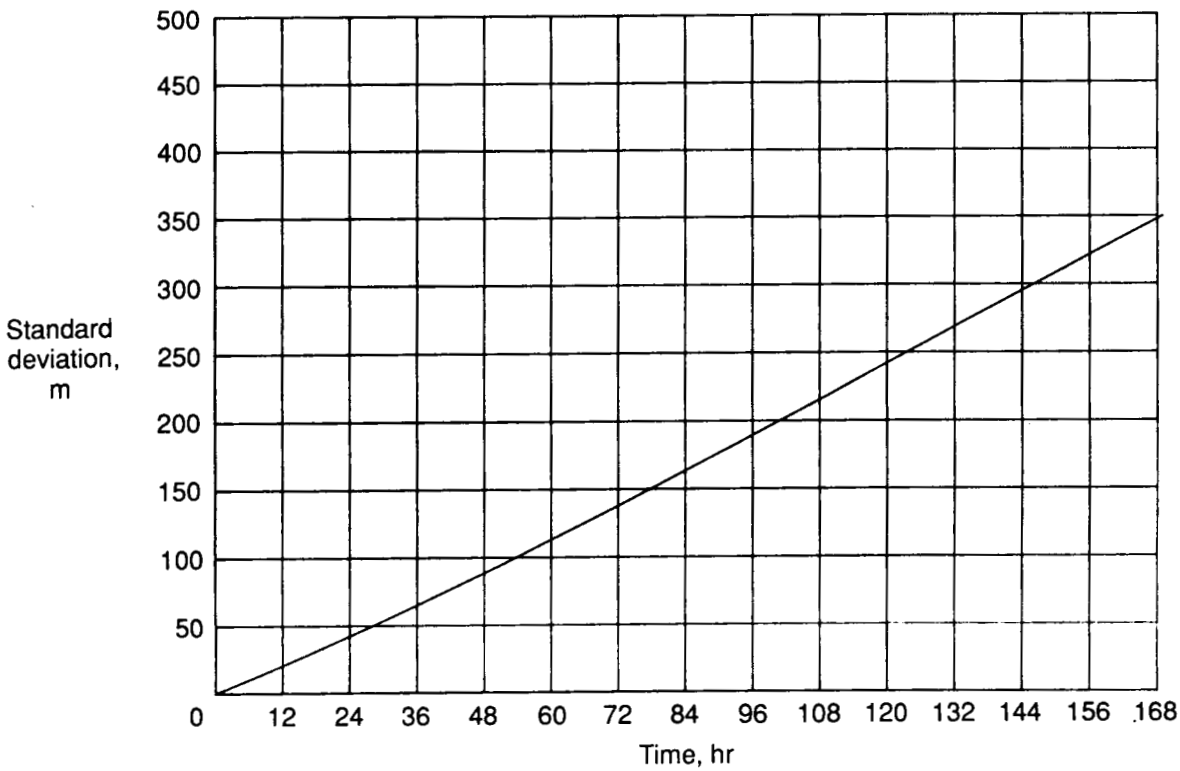

Figure 10. Same as figure 9 for the sunset altitude error.

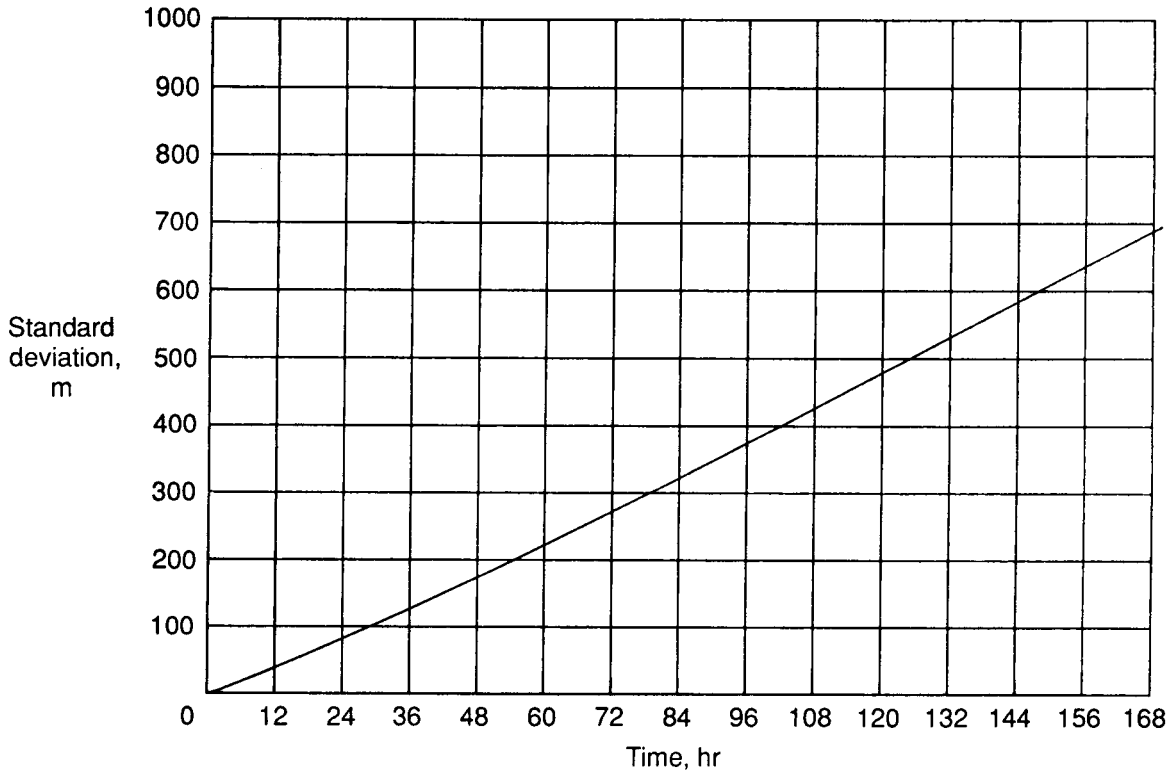

Figure 11. Same as figure 9 for the difference between sunrise and sunset altitudes on the same orbit.

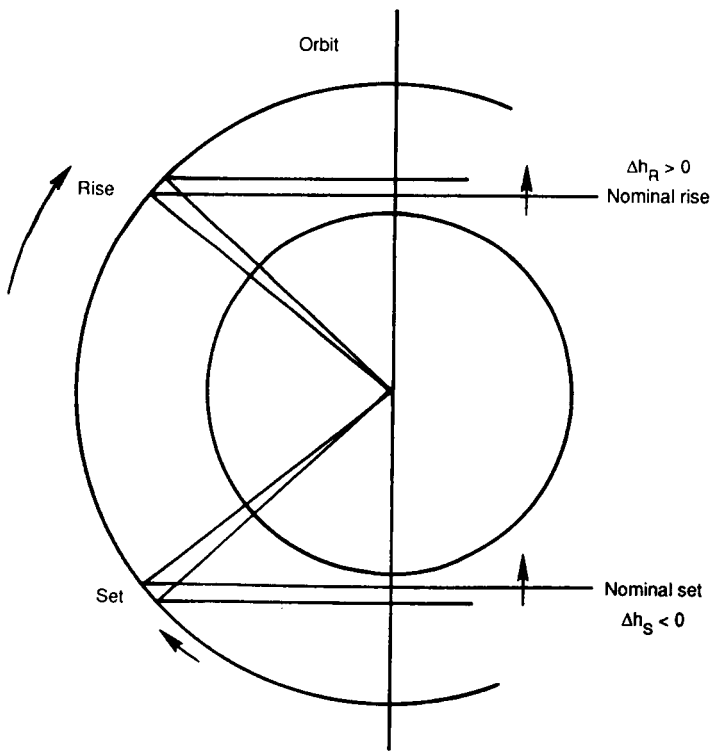

Figure 12. Sketch showing the increase in sunrise and decrease in sunset tangent point altitudes for a "fast" time error.

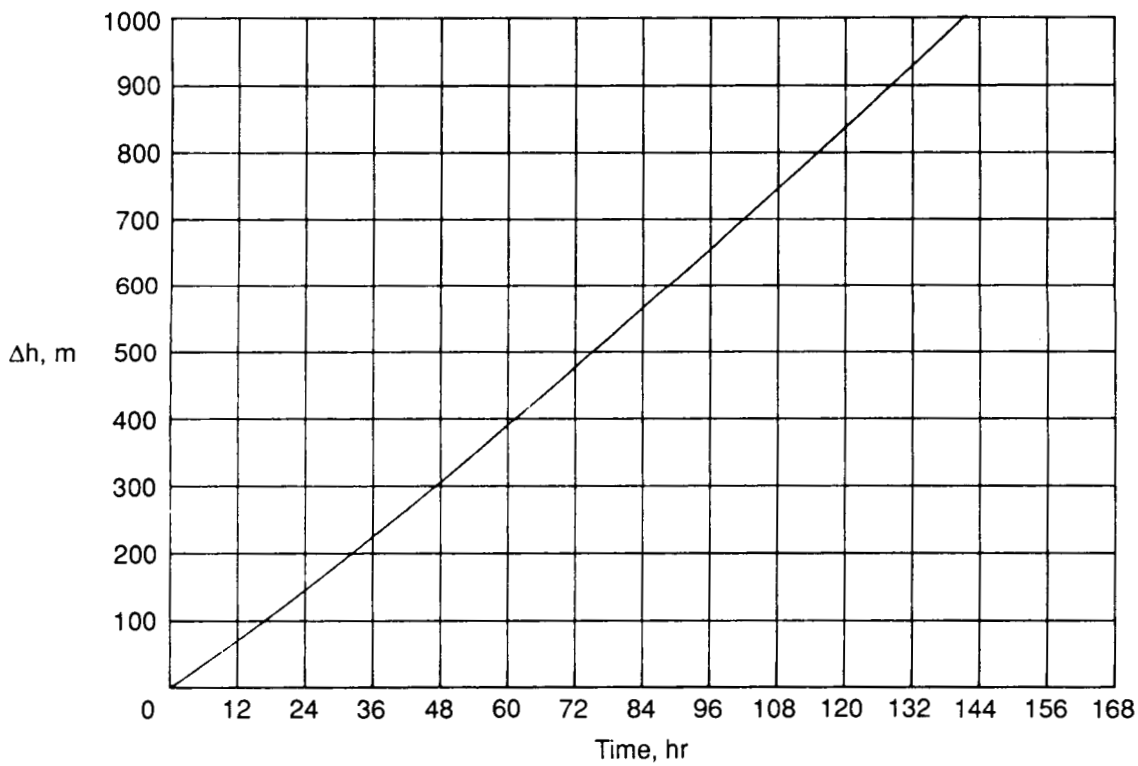

Figure 13. History of the difference between sunrise and sunset tangent point altitudes on 1 of the 100 perturbed orbits. For the week, the mean of the 100 runs was less than 10 m at 168 hr.

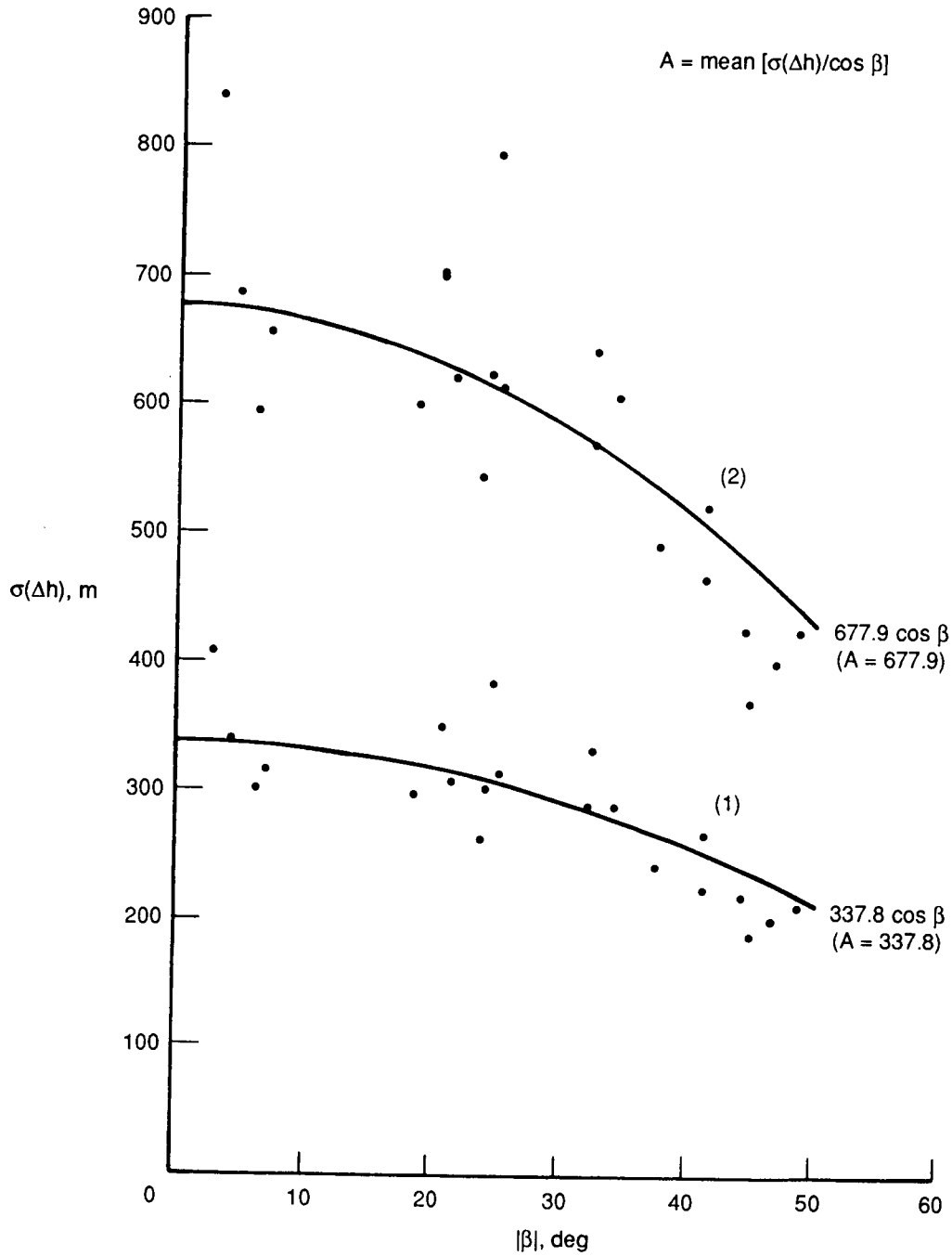

Figure 14. Effect of the β angle on the standard deviation in (1) the difference between the perturbed and nominal sunrise and sunset tangent point altitudes, and on (2) the difference between rise and set altitudes.

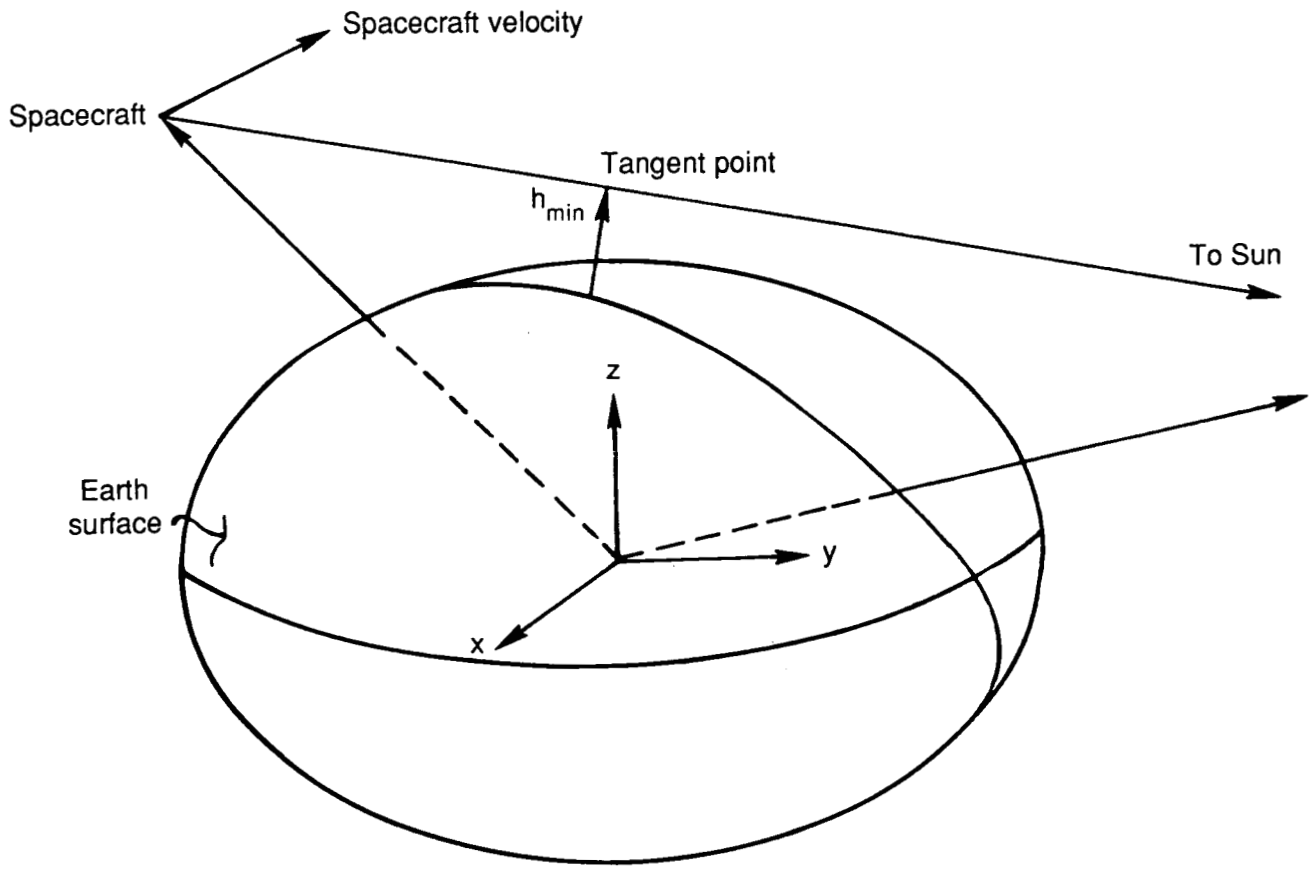

Figure 15. Geometry and definition of tangent point height.

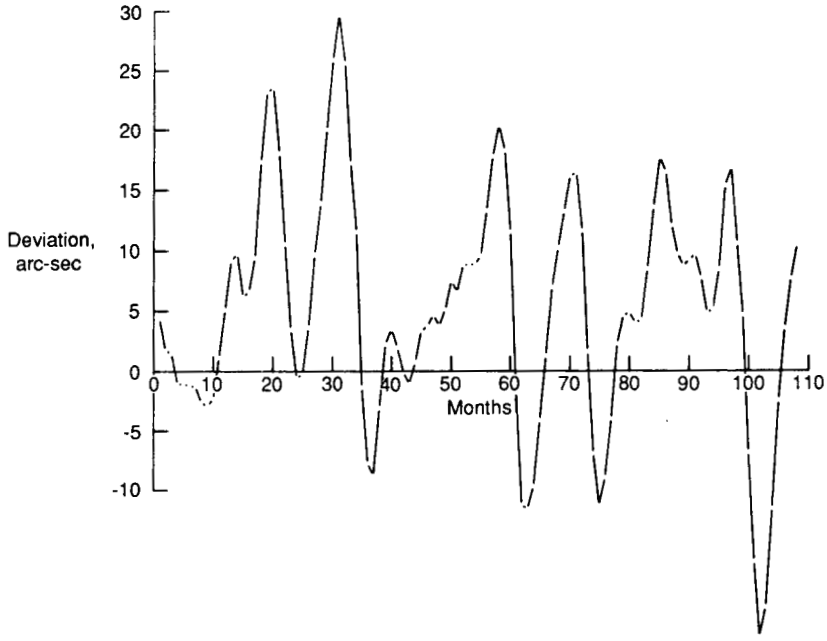

Figure 16. Difference between computed and published right ascension of the Sun, first of each month for the 9-year period 1979–1987 inclusive, arc-sec.

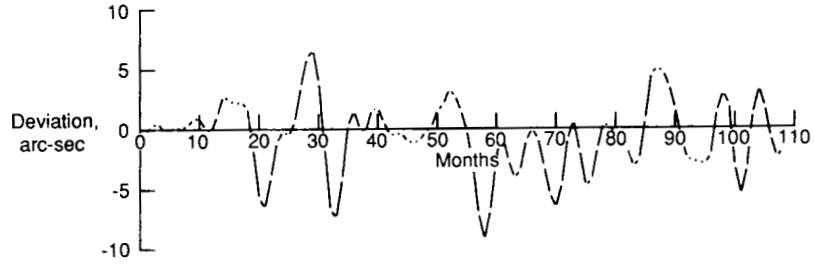

Figure 17. Difference between computed and published declination of the Sun, first of each month for the 9-year period 1979–1987, inclusive, arc-sec.

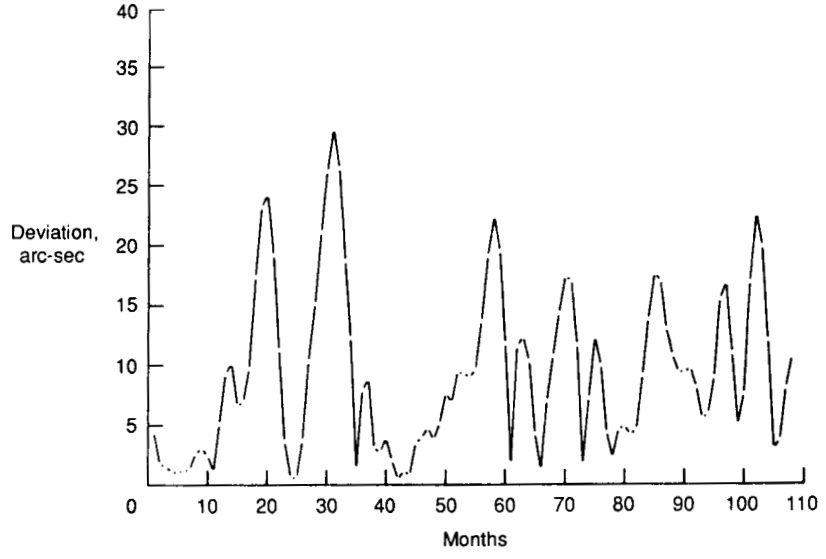

Figure 18. Plot of the quantity $[(\Delta ra)^2 + (\Delta dec)^2]^{1/2}$ for first day of each month for the 9-year period 1979–1987, inclusive, arc-sec.

Appendix A

Derivation of an Approximate Expression for the Standard Deviation in the Tangent Point Altitudes

If we assume nearly circular orbits and assume that $\beta = 0°$, then it is possible to derive an approximate expression for the standard deviation in the quantity $(h_R - h_{NR})$ or $(h_S - h_{NS})$ from figure 6(a). We will here call this quantity Δh, since to the degree of approximation used here, it is the same for both rise and set tangent point altitudes. From the figure

$$\Delta h = r_{sc,p} \sin \phi_p - r_{sc,N} \sin \phi_N \tag{A1}$$

where r_{sc} is the distance of the spacecraft from the Earth's center, and ϕ is defined as the angle from the local vertical to the center of the Sun. The angle θ (fig. 6(a)) is the angular distance between the nominal radius vector and the perturbed at the time at which the nominal vector reaches the position to produce the nominal value of the tangent point height. (Subscripts N and p refer to nominal and perturbed parameters, respectively.) If Δt is the time from the beginning of the computation period (zero time at the beginning of the tape), then approximately

$$\theta \approx \theta_o + (n_p - n_N)\Delta t \tag{A2}$$

where θ_o is the angular separation between the nominal and perturbed radius vectors at $t = 0$, and n is the mean angular rate in the orbit,

$$n^2 = \frac{\mu}{a^3} \tag{A3}$$

θ_o will generally be a very small angle (of the order of a few hundredths of an arc-sec) and hence will be neglected in what follows.

From figure 5,

$$\phi_N = \phi_p + \theta$$

Since the initial condition errors are very small, and the errors in the magnitude of the radius vector are very small (see fig. 15), then using equations (A3) and (A1) and assuming that $\theta << 1$ we get

$$\Delta h = -\theta \left(r_{sc,N} \cos \phi\right) \tag{A4}$$

The nominal value of n in equation (A2) is

$$n_N = \left(\frac{\mu}{a_N^3}\right)^{1/2}$$

where $\mu = 398\,600.64$ km^3/sec^2, the gravitational constant of the Earth, and a is the semimajor axis of the nominal orbit. If we expand n_p in a Taylor series about n_N,

$$n_p = n_N + \left(\frac{\partial n}{\partial a}\right)_N \Delta a + \ldots \tag{A5}$$

From equation (A3)

$$\frac{\partial n}{\partial a} = -\frac{3}{2}\frac{n_N}{a_N} \tag{A6}$$

and equation (A2) becomes

$$\theta = \left(\frac{3}{2}\frac{n_N}{a_N}\Delta a\right)\Delta t \tag{A7}$$

In terms of the magnitudes of the initial radius and velocity vectors,

$$\frac{1}{a_N} = \frac{2}{r_o} - \frac{v_o^2}{\mu} \tag{A8}$$

and hence

$$\left.\begin{aligned} \frac{\partial a}{\partial r_o} &= 2\left(\frac{a_N}{r_o}\right)^2 \\ \frac{\partial a}{\partial v_o} &= 2\frac{a_N^2 v_o}{\mu} \end{aligned}\right\} \tag{A9}$$

which gives

$$\begin{aligned} \Delta a &= \frac{\partial a}{\partial r_o}\Delta r_o + \frac{\partial a}{\partial v_o}\Delta v_o \\ &= 2\frac{a_N^2}{r_o^2}\Delta r_o + 2\frac{a_N^2 v_o}{\mu}\Delta v_o \end{aligned} \tag{A10}$$

Finally, with

$$\begin{aligned} r_o &= \left(x_o^2 + y_o^2 + z_o^2\right)^{1/2} \\ \Delta r_o &= \frac{\partial r_o}{\partial x_o}\Delta x_o + \frac{\partial r_o}{\partial y_o}\Delta y_o + \frac{\partial r_o}{\partial z_o}\Delta z_o \\ &= \frac{1}{r_o}\left(x_o\Delta x_o + y_o\Delta y_o + z_o\Delta z_o\right) \end{aligned} \tag{A11}$$

and similarly

$$\Delta v_o = \frac{1}{v_o}\left[\dot{x}_o\Delta\dot{x}_o + \dot{y}_o\Delta\dot{y}_o + \dot{z}_o\Delta\dot{z}_o\right] \tag{A12}$$

In equations (A4) and (A7), the only random variables are θ and Δa, respectively. Hence, if we

assume Gaussian distributions with zero means

$$\sigma(\Delta h) = |r_{sc,N} \cos \phi_N| \sigma(\theta) \tag{A13}$$

and

$$\sigma(\theta) = \left| \frac{3}{2} \frac{n_N}{a_N} \Delta t \right| \sigma(a) \tag{A14}$$

in which from equation (A10), assuming no correlation between initial position and initial velocity errors,

$$\sigma(a) = \left[\left(\frac{2a_N^2}{r_o^2} \right)^2 \sigma^2(r_o) + \left(\frac{2a_N^2 v_o}{\mu} \right)^2 \sigma^2(v_o) \right]^{1/2} \tag{A15}$$

and

$$\sigma(r_o) = \frac{1}{r_o} \left\{ [x_o \sigma(x_o)]^2 + [y_o \sigma(y_o)]^2 + [z_o \sigma(z_o)]^2 \right\}^{1/2} \tag{A16}$$

$$\sigma(v_o) = \frac{1}{v_o} \left\{ [\dot{x}_o \sigma(\dot{x}_o)]^2 + [\dot{y}_o \sigma(\dot{y}_o)]^2 + [\dot{z}_o \sigma(\dot{z}_o)]^2 \right\}^{1/2} \tag{A17}$$

If we make the assumption that

$$\sigma(x_o) = \sigma(y_o) = \sigma(z_o) = \sigma$$

with a similar expression for the velocity components, then equations (A16) and (A17) become simply

$$\sigma(r_o) = \sigma$$
$$\sigma(v_o) = \dot{\sigma}$$

when approximately

$$\sigma = \left\{ \frac{1}{3} \left[\sigma^2(x_o) + \sigma^2(y_o) + \sigma^2(z_o) \right] \right\}^{1/2}$$
$$\dot{\sigma} = \left\{ \frac{1}{3} \left[\sigma^2(\dot{x}_o) + \sigma^2(\dot{y}_o) + \sigma^2(\dot{z}_o) \right] \right\}^{1/2}$$

For SAGE I, we have nominally $a = 6980$ km and

$$\sigma = 3.32 \times 10^{-4} \text{ km}$$
$$\dot{\sigma} = 3.51 \times 10^{-7} \text{ km/sec}$$

which gives

$$\sigma(a) = 9.23 \times 10^{-4} \text{ km}$$
$$\sigma(\theta) = 1.3 \times 10^{-7} \text{ rad}$$
$$\sigma(\Delta h) = 369 \text{ m}$$

From equations (A13) and (A14) we see that, to the order of approximation introduced in this analysis, $\sigma(\Delta h)$ is a linear function of time, a conclusion that is approximately borne out in figures 9–11. The slight departure from nonlinearity in these figures is due to the variation in the β angle during the 7 days of error propagation. Identical plots for other time periods show that $\sigma(\Delta h)$ versus time is slightly concave upward when β decreases over the time period and slightly concave downward when β increases, showing that as β gets large the magnitude of the errors decreases, and vice versa, as heuristically developed in the text (see fig. 6).

Appendix B

Application of f and g Series to Error Propagation

The f and g series method can readily be used to develop analytic expressions for the propagation of errors along an orbit. These relations state that (see, e.g., Escobal 1965)

$$\mathbf{r}(t, t_o) = f(t, t_o)\mathbf{r}_o + g(t, t_o)\mathbf{v}_o \tag{B1}$$

where $\mathbf{r}(t)$ is the position vector at any time t, given in terms of the initial position vector $\mathbf{r}_o$ and the initial velocity vector $\mathbf{v}_o$. The f and g series are, in general, infinite series derived by expanding the radius vector in a Taylor series, replacing $\ddot{\mathbf{r}}$ by the expression for the acceleration due to gravity as soon as $\ddot{\mathbf{r}}$ appears, and collecting the coefficients of $\mathbf{r}_o$ (f series) and $\dot{\mathbf{r}}_o$ (g series). For the simple two-body problem, where the gravitational force of the attracting body is a central force, the f and g series can be expressed in exact closed form (Escobal 1965)

$$f(t, t_o) = 1 - \frac{a}{r_o}[1 - \cos(E - E_o)] \tag{B2}$$

$$g(t, t_o) = (t - t_o) - \frac{1}{n}[(E - E_o) - \sin(E - E_o)] \tag{B3}$$

in which a is the semimajor axis of the orbit, E_o and E are the initial and current values of eccentric anomaly, and n is the mean angular rate in the orbit

$$n^2 = \frac{\mu}{a^3} \tag{B4}$$

in which μ is the gravitational constant of the central body (for the Earth, $\mu = 398\,600.64$ km/sec).

For circular orbits, the f and g expressions reduce considerably, and, for example, the x-component of equation (B1) can be written as

$$x(t, t_o) = x_o \cos\, n(t - t_o) + \frac{\dot{x}_o}{n} \sin\, n(t - t_o) \tag{B5}$$

with similar expressions for y and z. These can in turn be differentiated to yield expressions for the velocity components. Only the x-component will be developed here.

Suppose now that uncertainties are introduced into the initial conditions $-\Delta x_o$, Δy_o, ..., $\Delta \dot{z}_o$. Equation (A10), with equations (A11) and (A12), still defines Δa. Then

$$\Delta x(t, t_o) = \frac{\partial x(t, t_o)}{\partial x_o}\Delta x_o + \frac{\partial x(t, t_o)}{\partial \dot{x}_o}\Delta \dot{x}_o + \frac{\partial x(t, t_o)}{\partial n}\frac{\partial n}{\partial a}\Delta a \tag{B6}$$

With the help of equation (B5) and a little algebra, we can write equation (B6) as

$$\Delta x(t, t_o) = A \sin(n\ \Delta t) + B\ \cos(n\ \Delta t) \tag{B7}$$

where

$$A = \left(\frac{\Delta \dot{x}_o}{n} + \frac{3}{2}\frac{\dot{x}_o}{n}\frac{\Delta a}{a}\right) + \left(\frac{3}{2} n x_o \frac{\Delta a}{a}\right)\Delta t \tag{B8}$$

$$B = \Delta x_o - \frac{3}{2}\dot{x}_o \frac{\Delta a}{a}\Delta t \tag{B9}$$

and Δa follows from the equations of appendix A already cited.

If we define

$$\tan \psi = \frac{B}{A} \tag{B10}$$

then we can write equation (B7) in the more compact form

$$\Delta x(t, t_o) = \sqrt{A^2 + B^2}\sin(n\,\Delta t + \psi) \tag{B11}$$

The variance $\sigma_x^2(t, t_o)$ does not assume such a simple form, and it is easier to evaluate it from the defining equation

$$\sigma_x^2(t, t_o) = \left(\frac{\partial x(t, t_o)}{\partial x_o}\sigma_{xo}\right)^2 + \left(\frac{\partial x(t, t_o)}{\partial \dot{x}_o}\sigma_{\dot{x}o}\right)^2 + \left(\frac{\partial x(t, t_o)}{\partial n}\frac{\partial n}{\partial a}\sigma_a\right)^2 \tag{B12}$$

Equations (B11) and (B12) were evaluated using the same initial conditions as were used to generate figure 13, along with the variances cited in the main text. The results from these two equations are plotted in figures B1 and B2, respectively. The similarity between figure 4 of the main text and figure B2 cannot be missed. The small differences are due to an inconsistency in the use of equations (B11) and (B12). The nominal Cartesian coordinates used in the definitions of the A and B parameters, equations (B8) and (B9), were the same as those used in generating the single orbit whose partial results are shown in figure 13. These nominal Cartesian coordinates do not produce quite a circular orbit, as assumed in the development of equations (B11) and (B12), but rather an orbit with an eccentricity of 0.00807. Consequently, $r_o \neq a$, and v_o is not the circular orbital velocity at radius a. These inconsistencies introduce small timing errors in the computation of the mean angular rate, which are mainly responsible for the differences between figures 4 and B2.

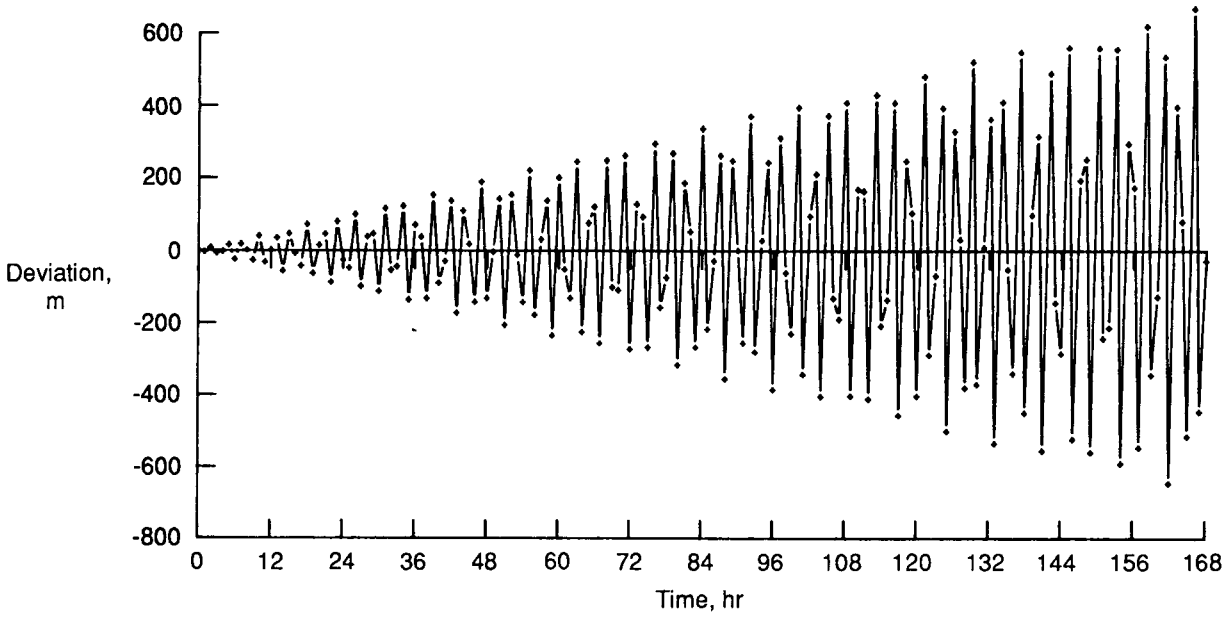

Figure B1. Analytic computation of the deviation in the x-component of spacecraft position due to initial perturbations equal to the standard deviations given in the text. Computed from equation (B11).

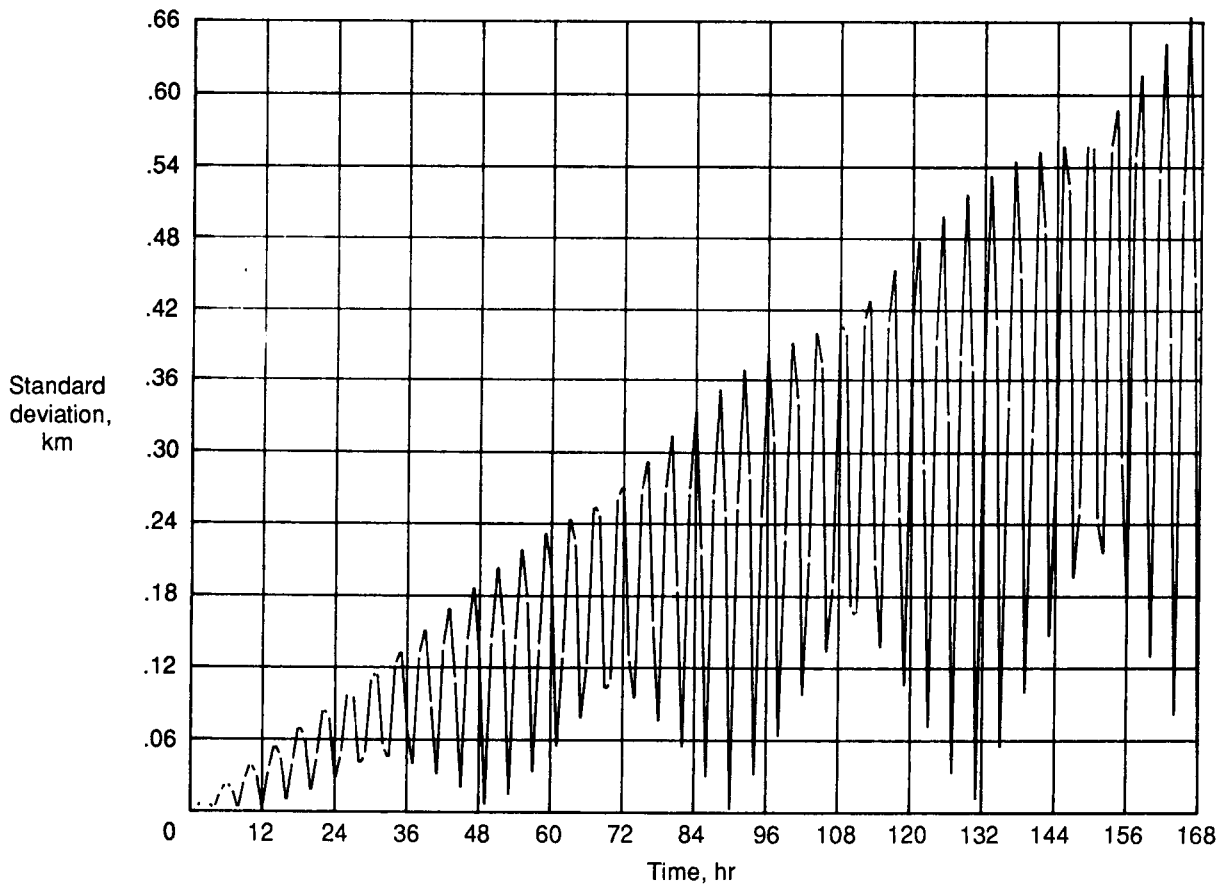

Figure B2. Same data as figure 4, but computed using the same inputs as in figure B1, and using equation (B12).

References

Buglia, James J.: *Direct Computation of Orbital Sunrise or Sunset Event Parameters.* NASA TM-87717, 1986.

Buglia, James J.: *Compilation of Methods in Orbital Mechanics and Solar Geometry.* NASA RP-1204, 1988.

Chu, William P.: Calculations of Atmospheric Refraction for Spacecraft Remote-Sensing Applications. *Appl. Opt.*, vol. 22, no. 5, Mar. 1, 1983, pp. 721–725.

Escobal, Pedro Ramon: *Methods of Orbit Determination.* John Wiley & Sons, Inc., c.1965.

Heiskanen, Weikko A.; and Moritz, Helmut: *Physical Geodesy.* W. H. Freeman & Co., c.1967.

Mauldin, L. E., III; Zaun, N. H.; McCormick, M. P., Jr.; Guy, J. H.; and Vaughn, W. R.: Stratospheric Aerosol and Gas Experiment II Instrument: A Functional Description. *Opt. Eng.*, vol. 24, no. 2, Mar./Apr. 1985, pp. 307–312.

McCormick, M. P.: Aerosol Measurements From Earth Orbiting Spacecraft. *Adv. Space Res.*, vol. 2, no. 5, 1982, pp. 73–86.

Smart, W. M. (revis. by R. M. Green): *Textbook on Spherical Astronomy,* Sixth ed. Cambridge Univ. Press, c.1977.

Taff, Laurence G.: *Celestial Mechanics.* John Wiley & Sons, Inc., c.1985.

NASA
National Aeronautics and Space Administration

Report Documentation Page

1. Report No.	2. Government Accession No.	3. Recipient's Catalog No.
NASA TP-2866		

4. Title and Subtitle	5. Report Date
Effect of Ephemeris Errors on the Accuracy of the Computation of the Tangent Point Altitude of a Solar Scanning Ray as Measured by the SAGE I and II Instruments	February 1989
	6. Performing Organization Code
7. Author(s)	8. Performing Organization Report No.
James J. Buglia	L-16485
9. Performing Organization Name and Address	10. Work Unit No.
NASA Langley Research Center Hampton, VA 23665-5225	665-45-30-21
	11. Contract or Grant No.
12. Sponsoring Agency Name and Address	13. Type of Report and Period Covered
National Aeronautics and Space Administration Washington, DC 20546-0001	Technical Paper
	14. Sponsoring Agency Code

15. Supplementary Notes

16. Abstract

An analysis was made of the error in the minimum altitude of a geometric ray from an orbiting spacecraft to the Sun. The dominant errors result from two sources: determining the position of the spacecraft and determining the position of the Sun. The sunrise and sunset errors are highly correlated and opposite in sign. With the ephemeris generated for the SAGE I instrument data reduction, these errors can be as large as 200–350 m (1σ) after 7 days of orbit propagation. The bulk of this error results from errors in the position of the orbiting spacecraft rather than errors in computing the position of the Sun. These errors, in turn, result from the discontinuities in the ephemeris tapes resulting from the orbital determination process. Data taken from the end of the "definitive" ephemeris tape are used to generate the "predict" data for the time interval covered by the next arc of the orbit determination process. The predicted data are then updated by using the tracking data. The growth of these errors is very nearly linear, with a slight nonlinearity caused by the beta angle. An approximate analytic method is given that predicts the magnitude of the errors and their growth in time with reasonable fidelity.

17. Key Words (Suggested by Authors(s))	18. Distribution Statement
Ephemeris Solar scanning ray	Unclassified—Unlimited Subject Category 64

19. Security Classif.(of this report)	20. Security Classif.(of this page)	21. No. of Pages	22. Price
Unclassified	Unclassified	27	A03

NASA FORM 1626 OCT 86

NASA-Langley, 1989

For sale by the National Technical Information Service, Springfield, Virginia 22161-2171